Delays and Oscillations in Networks of Spiking Neurons - a Two Time Scale Analysis

Dotan Di Castro[1], Ron Meir[1], Irad Yavneh[2]
Department of Electrical Engineering[1] and Computer Science[2]
Technion, Israel
August 10, 2008

Neural Computation, In Press

Abstract

Oscillations are a ubiquitous feature of many neural systems, spanning many orders of magnitude in frequency. One of the most prominent oscillatory patterns, with possible functional implications, is that occurring in the mammalian thalamo-cortical system during sleep. This system is characterized by relatively long delays (reaching up to 40 msec), and gives rise to low frequency oscillatory waves. Motivated by these phenomena, we study networks of excitatory and inhibitory integrate and fire neurons within a Fokker-Planck delay partial differential equation formalism, and establish explicit conditions for the emergence of oscillatory solutions, and for the amplitude and period of the ensuing oscillations, for relatively large values of the delays. By employing a two time scale analysis, the full partial differential equation is replaced in this limit by a discrete time iterative map, leading to a relatively simple dynamic interpretation. This asymptotic result is shown numerically to hold, to a good approximation, over a wide range of parameter values, leading to an accurate characterization of the behavior in terms of the underlying physical parameters. Our results provide a simple mechanistic explanation for one type of slow oscillation based on delayed inhibition, which may play an important role in the slow spindle oscillations occurring during sleep. Moreover, they are consistent with experimental findings related to human motor behavior with visual feedback.

1 Introduction

Neuronal oscillations in cortical networks, spanning five orders of magnitude in frequency (Buzsáki, 2006; Buzsáki & Draguhn, 2004), are playing an increasingly important role in attempts to interpret the behavior of mammalian nervous systems. A particularly prominent role is played by the many rhythms characterizing the sleep state, which have been suggested to be implicated in input gating, neuronal assembly construction, facilitation of synaptic plasticity and long-term consolidation (e.g., (Buzsáki, 2006; Buzsáki & Draguhn, 2004)). Among the many types of sleep oscillations a particularly prominent role is played by the so-called spindle oscillations (in the range of $12-20$ Hz), generated within the thalamocortical system, which are synchronized over large cortical regions. In vivo experiments have demonstrated the critical involvement of the inhibitory neurons from the reticular nucleus of the thalamus (Buzsáki, 2006), rather than local-circuit interneurons. An important characteristic of this thalamocortical-reticular system is the longer delays required for information to propagate from the cortex to the thalamus and reticular nucleus. For example, (Ferster & Lindström, 1983; Harvey, 1980; Miller, 1996; Swadlow, 1991) provide experimental evidence that cortico-thalamic projections originating in layer 6 of the cortex have conduction times up to 40 msec; see also Buzsáki (Buzsáki, 2006). These delays are much longer than the characteristic neuronal time scales, which are in the order of several milliseconds. The model developed in this paper is motivated by this time scale separation, which leads to an analytically tractable and accurate description of large scale oscillations in the regime where the temporal delays are long. Interestingly, this framework provides a good description of oscillations in other regimes as well.

While several detailed and physiologically motivated models have been proposed to explain the origin of spindle oscillations (Destexhe, Contreras, & Steriade, 1998; Hill & Tononi, 2005), incorporating many details at the level of both single neurons, synapses and networks, we propose a simple model for networks of excitatory and inhibitory neurons, influencing each other through delayed synaptic interactions. Several previous models have dealt with the effect of delayed inhibition on the generation of global network oscillations (e.g., (Brunel, 2000; Brunel & Hakim, 1999; Lindner, Doiron, & Longtin, 2005; Marinazzo, Kappen, & Gielen, 2007)). The main contribution of the present work is in deriving an explicit discrete time dynamic recursion for the oscillatory dynamics, enabling a straightforward analysis in terms of phase plane tools. Moreover, we obtain closed form analytic expressions for the various oscillation parameters, which depend explicitly on the neuronal and network parameters, thereby relating microscopic variables to the emergent dynamic behavior. A specific

prediction of our model is that the oscillation period is given by twice the delay period. For delays in the range of $20 - 40$ milliseconds this implies oscillation frequencies of $12.5 - 25$ Hz, well within the range of the spindle oscillation frequencies. While we do not expect our model to replace the detailed models developed so far (e.g., (Destexhe et al., 1998; Hill & Tononi, 2005)), it does serve to provide a relatively simple and direct explanation for global oscillations based on delayed feedback inhibition.

Systems composed of nonlinearly interacting elements, e.g., neurons and synapses, constitute basic building blocks of the information processing and computation that is believed to take place in the cerebral cortex. While the behavior of single such elements, receiving external stochastic input, has been mathematically analyzed and characterized over many years (e.g., (Tuckwell, 1989)), combining spiking neurons into a network of interacting elements poses very challenging mathematical problems, many of which are still open. In particular, viewing such networks as input/output systems in the engineering sense of the word, a basic issue relates to determining the relationship between the input to the system and the output resulting from the stochastic nonlinear dynamics. Characterizing such a relationship is essential if one is aiming at understanding more complex structures composed of multiple systems. While a large variety of model neurons exists, in this work we use the simple Leaky Integrate and Fire (LIF) model neuron, which has played a particularly important role in neural modeling, in spite of its limitations (e.g., (Gerstner & Kistler, 2002; Vogels, Rajan, & Abbott, 2005)).

It has been known for a long time that delayed inhibition can result in oscillations (Glass & Mackey, 1988; Murray, 2002). However, the precise interplay between internal feedback and the driving force has not been widely studied. The main contribution of this work is the formulation of explicit physically meaningful conditions for the onset of oscillations, and for their frequencies and amplitudes. We consider populations of LIF neurons interacting through temporal delays, described within the classic Fokker-Planck (FP) partial differential equation (PDE) framework (Risken, 1996). Our explicit results are precise in well-defined limits, and are shown by careful numerical solutions of the PDE to hold approximately across a broad range of the physical parameters.

While much previous work was devoted to a mean field approach to populations of spiking neurons (see (Renart, Brunel, & Wang, 2003) for an extensive review), most of the work on the emergence of oscillatory solutions has been either numerical (e.g., (White, Chow, Ritt, Soto-Trevio, & Kopell, 1998)), or based on linear stability analysis (e.g., (Brunel, 2000; Brunel & Hakim, 1999; Lindner et al., 2005)), which is often hard to interpret in direct

physical terms. Moreover, the case of delays has not been considered extensively. In this context, (Brunel & Hakim, 1999) studied a population of integrate and fire inhibitory neurons, and demonstrated, using linear stability analysis, a sharp transition from irregular firing to synchronized oscillatory activity. Roxin et al. (Roxin, Brunel, & Hansel, 2005) investigated the role of delays in rate-based Wilson-Cowan type systems with spatial structure, interacting via delayed excitatory and inhibitory interactions. While many of their results were analogous to those displayed in simulations of spiking neurons, they were not directly derived from the spiking neuron dynamics. A more detailed comparison with (Brunel & Hakim, 1999) is presented in Section 3.1. Finally, (Lindner et al., 2005) and (Marinazzo et al., 2007) also considered the effect of delayed inhibition on network oscillations. However, they studied a two-layered architecture of excitatory and inhibitory neurons, without lateral interactions within each population. Similarly to (Brunel & Hakim, 1999) their derivation of conditions for oscillations was also based on linear response theory. Related work in (Börgers & Kopell, 2003) also discusses the effects of different temporal scales (rather than delays) on oscillations.

We stress that our main aim here is to develop a concise mathematical characterization of the effect of inhibition and long delays on network behavior, rather than on studying precise architectural details. Such a description can form the basis for more extensive studies involving detailed architectural constraints and specific experimental conditions.

The remainder of this paper is organized as follows. We begin in Section 2 with a statement of the problem and the equations describing the system. An important step facilitating further analysis is based on recasting the underlying equations in dimensionless form. Section 3.1 presents a two-time-scale analysis of the problem in the limit of large delays, demonstrating how it can be approximated by a discrete recursive mapping. This section also presents some qualitative and quantitative predictions of the model, and compares them to a careful numerical solution of the full PDE. The details of the somewhat non-standard numerical solution scheme are presented in Appendix B. Section 3.2 presents another special limit, corresponding to low diffusion, where an approximate characterization of the oscillation can be derived analytically. The paper concludes in Section 4 with a summary of the results and a short discussion.

2 Problem Formulation

In this section, and in the sequel, we follow the notation and nomenclature of (Brunel, 2000). For completeness, we repeat the main steps in the derivation of the network level Fokker-Planck equation.

2.1 The Model

We consider a system of N LIF neurons, composed of N_E excitatory neurons and N_I inhibitory neurons, where $N = N_E + N_I$. The voltage dynamics of each neuron is given by the following stochastic differential equation complemented by a threshold condition

$$\begin{cases} \tau_i \dfrac{d}{dt} v_i(t) = -v_i(t) + R_i I_i(t) + z_i(t), \\ \text{if } v = \theta \text{ then } v_i = v_r \text{ for } \tau_{\text{ref}} \text{ seconds}, \end{cases}$$

where τ_i is the membrane time constant, $I_i(t)$ is the input current received from other neurons, and $z_i(t)$ represents a noisy external input, assumed for simplicity to be Gaussian white noise with mean μ_e and variance σ_e^2. The parameter θ is a threshold for generating a spike, upon which the voltage is reset to v_r for τ_{ref} seconds. The input current $I_i(t)$ is given by

$$RI_i(t) = \sum_{j=1, j\neq i}^{C_i} J_{ij} \sum_k \delta(t - t_j^k - D_{ij}), \quad i = 1, 2, \ldots, N,$$

where C_i represents the number of inputs to the ith neuron, J_{ij} is the strength of the connection between the jth presynaptic neuron and the ith postsynaptic neuron, $\{t_j^k\}_k$ are the firing times of the jth pre-synaptic neuron, and D_{ij} is the propagation delay between the jth neuron and the ith neuron. We consider two *homogeneous* populations of excitatory and inhibitory neurons, where $J_{ij} = J_E > 0$ if j is an excitatory neuron, and $J_{ij} = J_I < 0$ if j is inhibitory. Based on the homogeneity assumption, we take all delays to be equal, namely $D_{ij} = D$ for all i and j, and $\tau_i = \tau$ for all i. The input to each cell consists of C_E excitatory neurons and C_I inhibitory currents where $C_E + C_I = C$, and we set $g = |J_I|/J_E$, and $\gamma = C_I/C_E$.

Brunel (Brunel, 2000) shows that in the limit $N_E, N_I \to \infty$, with $C_E/N_E \to 0$ and $C_I/N_I \to 0$, one obtains a FP Equation (Risken, 1996). The FP equation is a partial differential equation, describing the evolution in time of the probability density function $P(v, t)$. The function $P(v, t)dv$ describes the probability of finding the membrane within

the voltage range $[v, v+dv]$ at time t. According to (Brunel, 2000) the FP equation and boundary conditions for a network of LIF neurons is

$$\begin{cases} \dfrac{\partial P(v,t)}{\partial t} = -\dfrac{\partial S(v,t)}{\partial v} + \delta(v-v_r)S(\theta,t), \\ S(v,t) = -\left[\dfrac{v}{\tau} - \dfrac{\mu_e}{\tau} - C_E J_E(1-\gamma g)S(\theta,t-D)\right] P(v,t) \\ \qquad\qquad - \left[\dfrac{\sigma_e^2}{\tau} + C_E J_E^2(1+\gamma g^2)S(\theta,t-D)\right] \dfrac{\partial P(v,t)}{\partial v}, \\ P(\theta,t) = 0, \\ P(-\infty,t) = 0, \\ P(v,0) = h(v) \quad \text{where} \quad \displaystyle\int_{-\infty}^{\theta} h(v)dv = 1. \end{cases} \tag{1}$$

Here $S(v,t)$ is the probability flux through v at time t. Without loss of generality, we assume that the initial time is $t=0$. The second term in the definition of $S(v,t)$ leads to what is often termed the diffusion term of the PDE. For simplicity, we have set $\tau_{\text{ref}} = 0$, and replaced the boundary condition stated in (Brunel, 2000) at $v = v_r$ with a singular contribution $\delta(v-v_r)S(\theta,t)$. This representation is mathematically equivalent, but more convenient for solving the FP equation numerically. Also, it expresses more explicitly the fact that the probability flux leaving the domain is injected at $v = v_r$. We note that setting $\tau_{\text{ref}} = 0$ does not modify our results significantly, so long as $\tau_{\text{ref}} \ll \tau_e$, where τ_e is defined in (3) below.

We define the network *activity*, $\nu(t)$, as the probability flux per unit time (Brunel, 2000), given by

$$\nu(t) \triangleq S(\theta,t) = -\left[\frac{\sigma_e^2}{\tau} + C_E J_E^2(1+\gamma g^2)\nu(t-D)\right] \frac{\partial P(v,t)}{\partial v}\bigg|_{v=\theta}. \tag{2}$$

Keeping in mind that $S(v,t)$ in (1) depends on $P(v,t)$ it is clear that (1) is not a linear PDE. More precisely, (1) is a quasi-linear elliptic delay PDE. While there is no known closed form solution to this type of PDE, it can be studied analytically in certain physically meaningful limits. In particular, our main focus in this work is on the oscillatory regime, which has mainly been studied through simulations in the past. More specifically, we consider two regimes where significant analytic advances can be made.

1. The regime of large temporal delays, which, when combined with a dominant inhibitory component is known to lead to oscillations (Glass & Mackey, 1988; Murray, 2002). The basic observation here is that for large temporal delays we can separate the dynamics into two distinct time scales. The first temporal scale leads to fast relaxation into a

quasi-steady mode with a characteristic time scale of the (large) delay D; see Section 3.1 for details.

2. The regime where the external input is characterized by a large mean and a small variance, and where the internal feedback variance is also small. This regime corresponds to a low diffusion level. In this case oscillations occur even for small delays, and their properties can be described accurately within our framework; see Section 3.2 for details.

2.2 A dimensionless FP equation

The analysis of (1) is greatly facilitated by expressing it in a *dimensionless* form. In this section we use hats above symbols to denote dimensionless variables. First, we define a characteristic time, τ_e, related to the system's response to the external input,

$$\tau_e \stackrel{\triangle}{=} \frac{\tau}{(\mu_e - v_r)/(\theta - v_r)}. \tag{3}$$

The variable τ_e relates the characteristic membrane time scale τ to the expected strength of the external driving force μ_e, and is related to the typical response time of an externally driven system. We assume throughout that $\tau_e \geq 0$.

Observe that $P(v,t)$ has the dimensions of volt^{-1}, while S has the dimensions of sec^{-1}. We define the following *dimensionless* variables

$$\hat{v} \stackrel{\triangle}{=} \frac{v - v_r}{\theta - v_r}, \quad \hat{t} \stackrel{\triangle}{=} \frac{t}{D}, \quad \hat{P}(v,t) \stackrel{\triangle}{=} (\theta - v_r)P(\hat{v},\hat{t}), \quad \hat{S}(\hat{v},\hat{t}) \stackrel{\triangle}{=} \tau_e S(v,t), \tag{4}$$

and an additional dimensionless parameter that represents a ratio of time scales,

$$\hat{\epsilon} \stackrel{\triangle}{=} \frac{\tau_e}{D}. \tag{5}$$

Note that the dimensionless reset value is $\hat{v} = 0$ and the dimensionless threshold value is $\hat{v} = 1$.

Substituting (3), (4), and (5) into (1), we obtain the following dimensionless equations

and boundary conditions

$$\begin{cases} \hat{\epsilon}\dfrac{\partial \hat{P}(\hat{v},\hat{t})}{\partial \hat{t}} = -\dfrac{\partial \hat{S}(\hat{v},\hat{t})}{\partial \hat{v}} + \delta(\hat{v})\hat{S}(1,\hat{t}) \ , \\ \quad \hat{S}(\hat{v},\hat{t}) = -\left[\eta\hat{v} - 1 - \rho\hat{S}(1,\hat{t}-1)\right]\hat{P}(\hat{v},\hat{t}) - \left[\eta\beta + \kappa\hat{S}(1,\hat{t}-1)\right]\dfrac{\partial \hat{P}(\hat{v},\hat{t})}{\partial v} \ , \\ \quad \hat{P}(1,\hat{t}) = 0, \\ \hat{P}(-\infty,\hat{t}) = 0, \\ \quad \hat{P}(v,0) = \hat{h}(\hat{v}) \quad \text{and} \quad \displaystyle\int_{-\infty}^{1} \hat{h}(\hat{v})d\hat{v} = 1 \ , \end{cases} \tag{6}$$

where we have introduced the following *dimensionless* parameters

$$\eta \triangleq \frac{\tau_e}{\tau}, \quad \rho \triangleq \frac{J_E C_E(1-\gamma g)}{\theta - v_r}, \quad \beta \triangleq \frac{\sigma_e^2}{(\theta - v_r)^2}, \quad \kappa \triangleq \frac{1}{2}\frac{J_E^2 C_E(1+\gamma^2 g)}{(\theta - v_r)^2}. \tag{7}$$

It is useful to interpret these parameters in physical terms.

- η is a time scale ratio, relating τ_e, the temporal response scale to an external stimulus, to the natural membrane time scale τ. Since τ_e is inversely proportional to μ_e, small values of η correspond a large external drive.
- ρ represents the normalized average network feedback, and can be either positive (dominant excitation) or negative (dominant inhibition).
- β is the normalized variance of the external noise process $z(t)$.
- κ is the normalized feedback variance, namely the variance resulting from the stochasticity of the neurons themselves.

The parameters η and β represent, respectively, the inverse mean and the variance of the external drive. Values of $\eta\beta \ll 1$ represent a focused driving force (large mean and small variance), while $\eta\beta \gg 1$ represents a diffuse drive. The variable κ is similar to β, except that it refers to the *internal* rather than to the external drive, whereas the variable ρ represents the internal (excitatory or inhibitory) drive, with large values corresponding to a strong internal drive. As can be expected, the dynamics of the system depends strongly on the balance between the values of these four parameters.

The dimensionless activity $\hat{\nu}(\hat{t})$ is given by

$$\hat{\nu}(\hat{t}) = \hat{S}(1,\hat{t}) = -[\eta\beta + \kappa\hat{\nu}(t-1)]\left.\frac{\partial \hat{P}(\hat{v},\hat{t})}{\partial \hat{v}}\right|_{\hat{v}=1} . \tag{8}$$

A remark concerning notation In this section we have used hats to denote dimensionless variables. In the sequel we use dimensionless variables throughout, and remove the hats in order to simplify the presentation. At specific points we will return to dimensional physical variables, and will indicate this explicitly.

3 Regimes Conducive to Oscillatory Solutions

Our main goal is to derive solutions describing oscillatory behavior. There are two main factors that are conducive to oscillatory solutions: relatively long delays and a strong and focused external drive (see also (Lindner et al., 2005)). It is well known that long delays tend to destabilize dynamical systems (e.g., (Murray, 2002)). The focused external driving force tends to synchronize the elements encouraging them to fire together. As demonstrated in (Lindner et al., 2005), for a different network architecture, single elements which are themselves oscillatory (such as LIF neurons subject to a focused external drive) tend to synchronize and oscillate under these conditions. We next study these factors as two separate regimes, and derive closed-form solutions in the limiting case for each one of them. These solutions are then shown numerically to be relevant across a rather wide range of parameters. The upshot is that these physically-meaningful results appear to yield at least a qualitative indication of the behavior whenever significantly oscillatory solutions exist, which becomes quantitatively accurate as the most strongly oscillatory regimes are approached.

3.1 The Regime of Long Delays

We begin with the case where the temporal delays are large relative to the characteristic neuronal time scales. In this case we use a two time scale analysis that enables us to replace the full PDE with a simple discrete recursion, which captures, in a simplified manner, the main features of the solution. A related neural network model with time scale separation was considered in (Cortes, Torres, Marro, Garrido, & Kappen, 2006), where presynaptic noise occurred on a time scale which was much shorter than the neural dynamics itself. Similarly to our case, this separation fasciated an approximate analytic treatment of the dynamics, although their neural model is very different from ours.

Before proceeding, we remind the reader that the variables and parameters in the sequel are all assumed to be dimensionless.

Consider an auxiliary *linear* PDE, which will be used in order to characterize the solution of the nonlinear PDE (6):

$$\begin{cases} \epsilon \dfrac{\partial P(v,t)}{\partial t} = -\dfrac{\partial S(v,t)}{\partial v} + \delta(1,t) S(1,t), \\ \quad S(v,t) = -\left[Av - B\right] P(v,t) - \dfrac{\partial P(v,t)}{\partial v}, \\ \quad P(1,t) = 0, \\ P(-\infty,t) = 0, \\ \quad P(v,0) = h(v) \qquad \text{and} \quad \displaystyle\int_{-\infty}^{1} h(v)dv = 1, \end{cases} \tag{9}$$

where $A \geq 0$ and B are real-valued parameters. This PDE possesses a steady state solution, P_{steady}, obtained by setting the left hand side of the first equation in (9) to zero. We find that

$$P_{\text{steady}}(v) = \begin{cases} \alpha e^{-\frac{(Av-B)^2}{2A}} & \text{if } v \leq 0 \ , \\ \alpha e^{-\frac{(Av-B)^2}{2A}} \left[\frac{\text{erfi}\left(\frac{A-B}{\sqrt{2A}}\right) - \text{erfi}\left(\frac{Av-B}{\sqrt{2A}}\right)}{\text{erfi}\left(\frac{A-B}{\sqrt{2A}}\right) - \text{erfi}\left(\frac{-B}{\sqrt{2A}}\right)} \right] & \text{otherwise} \ , \end{cases} \tag{10}$$

where

$$\text{erfi}(x) = \frac{\text{erfi}(ix)}{i}, \quad i = \sqrt{-1},$$

and where the constant α is determined from the normalization of the integral of P in (9). This normalization can be seen to remain valid for all time by integrating the equation over the v domain and using $S(-\infty, t) = 0$. Since ϵ, defined in (5), can be considered as a scaling of the time, the convergence rate of $P(v,t)$ to $P_{\text{steady}}(v)$ is proportional to $1/\epsilon$. For the case where $\epsilon \to 0$ the convergence is instantaneous. We use this fact to study the complete problem. For $\epsilon \to 0$, we assume that the solution to (6) is dominated by a quasi-steady (slowly varying) solution $P_0(v,t)$, with a characteristic time scale of 1 (or D in the dimensional system). The first approximation, neglecting the $O(\epsilon)$ term, leads to the following ordinary differential equation for $P_0(v,t)$

$$\begin{cases} 0 = -\dfrac{\partial S_0(v,t)}{\partial v} + \delta(1,t)\ S_0(1,t)\ , \\ S_0(v,t) = -\left[\eta v - 1 - \rho S_0(1,t-1)\right] P_0(v,t) - \left[\eta\beta + \kappa S_0(1,\ t-1)\right] \dfrac{\partial P_0(v,t)}{\partial v}\ , \\ P_0(1,t) = 0, \\ P_0(-\infty,t) = 0\ , \\ \displaystyle\int_{-\infty}^{1} P_0(v,t)dv = 1\ . \end{cases} \tag{11}$$

Given $S_0(1,t-1)$ and the fixed parameters η, ρ, β, and κ, the solution $P_0(v,t)$ can immediately be read from (10), by substituting

$$A = \frac{\eta}{\eta\beta + \kappa S_0(1,t-1)}, \quad B = \frac{1+\rho S_0(1,t-1)}{\eta\beta + \kappa S_0(1,t-1)} \; . \tag{12}$$

From (10) and (12) we can compute $\partial P_0/\partial v$ at $v=1$, which, combined with (9) and (11), leads to

$$\begin{aligned} -\left.\frac{\partial P_0(v,t)}{\partial v}\right|_{v=1} = \Bigg\{ & \frac{\pi}{2A}\mathrm{erfc}\left(\frac{B}{\sqrt{2A}}\right)\left[\mathrm{erfi}\left(\frac{A-B}{\sqrt{2A}}\right)+\mathrm{erfi}\left(\frac{B}{\sqrt{2A}}\right)\right] \\ & + \sqrt{\frac{\pi}{2A}}\int_0^1 e^{-\frac{(Au-B)^2}{2A}}\left[\mathrm{erfi}\left(\frac{A-B}{\sqrt{2A}}\right)+\mathrm{erfi}\left(\frac{Au-B}{\sqrt{2A}}\right)\right]du\Bigg\}^{-1} \; . \end{aligned} \tag{13}$$

Next, define $\nu_{\mathrm{new}} \stackrel{\triangle}{=} S_0(1,t)$ and $\nu_{\mathrm{old}} \stackrel{\triangle}{=} S_0(1,t-1)$. The relation between ν_{new} and ν_{old},

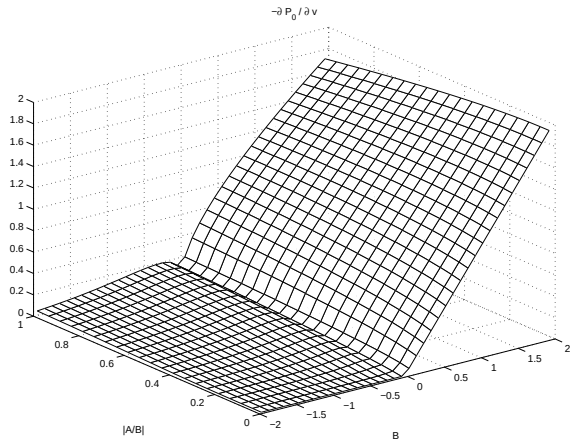

Figure 1: The behavior of the partial derivative $-\left.\frac{\partial P_0(v,t)}{\partial v}\right|_{v=1}$ vs. the parameters $|A/B|$ and B, from which the probability flux $\nu(t) = S_0(1,t)$ can be determined based on (8).

derived from (11) using $P_0(1,t)=0$, is given by

$$\nu_{\mathrm{new}} = G(\nu_{\mathrm{old}}) \qquad \text{where} \quad G(\nu_{\mathrm{old}}) \stackrel{\triangle}{=} -[\eta\beta + \kappa\nu_{\mathrm{old}}]\left.\frac{\partial P_0(v,t)}{\partial v}\right|_{v=1} \; . \tag{14}$$

Equation (14) can be viewed as a non-linear map $\nu_{\mathrm{old}} \mapsto \nu_{\mathrm{new}}$, where the steady state $\nu_{\mathrm{steady}} = \nu_{\mathrm{new}} = \nu_{\mathrm{old}}$ is obtained by setting $\nu_{\mathrm{steady}} = G(\nu_{\mathrm{steady}})$. This fixed point loses stability (Strogatz, 2001) when the condition

$$\left.\frac{d\nu_{\mathrm{new}}}{d\nu_{\mathrm{old}}}\right|_{\nu_{\mathrm{old}}=\nu_{\mathrm{steady}}} < -1 \tag{15}$$

is satisfied.

The only special assumption made so far in the two-timescale analysis is that ϵ is small, or, equivalently, the delay D is large. The mapping (14) is indeed *exact* in this limit. Deeper physical insight and simple closed form expressions can be obtained in the regime where the external driving force is characterized by a relatively large mean value (small η), and the relative variance - both internal and external - is not too large. The limiting case of this regime, where the variance is vanishingly small, will be studied separately in Section 3.2. Presently, we study the intersection between the regimes (where the oscillatory behavior is in fact strongest.) From (12) we have

$$\frac{A}{B} = \frac{\eta}{1+\rho\nu_{\text{old}}}\,. \tag{16}$$

When this term is small (i.e., the external drive is relatively strong), and $|B|$ is not too small (i.e., the system is not very diffusive), we can expand (14) in a power series, and obtain accurate approximations by taking just a few leading-order terms. Full details are given in Appendix A. Formally, the expansion is valid as long as

$$\eta < 1+\rho\nu_{\text{old}} \quad \text{and} \quad \kappa < \frac{(1+\rho\nu_{\text{old}}-\eta)^2 - 2\beta\eta^2}{2\eta\nu_{\text{old}}}, \tag{17}$$

whereupon the arguments of the error functions in (13) (i.e., erfi(x), erfc(x), and erfi(x)) are all larger than one. We focus on the leading terms, namely, the lowest orders in η. After some algebra we obtain for positive B

$$\nu_{\text{new}} = 1+\rho\nu_{\text{old}} - \frac{\eta}{2} - \frac{\eta\kappa\nu_{\text{old}}}{1+\rho\nu_{\text{old}}} - \frac{1-12\beta}{12(1+\rho\nu_{\text{old}})}\eta^2 + O(\eta^3+\kappa\eta^2). \tag{18}$$

When B (hence also $1+\rho\nu_{\text{old}}$) is negative, ν_{new} tends to zero exponentially fast as $\eta \to 0$.

To demonstrate the relevance of taking a few leading-order terms in the expansion , we plot $\partial P_0(v,t)/\partial v|_{v=1}$ against $(|A/B|, B)$, in Figure 1. It is readily seen that, as long as $|B|$ is not too small, the function behaves very smoothly, and, clearly, for $B<0$ it tends to 0 very fast when $|A/B|$ is small. More detailed statements regarding the series approximation appear in Appendix A.

3.1.1 Analysis

Several conclusions can be drawn immediately from (15) and (18).

- The steady state solution, given by setting $\nu_{\text{steady}} = G(\nu_{\text{steady}})$, yields, to leading order (in physical units), $\nu_{\text{steady}} = (\mu_e - (v_r + \theta))/(2\tau(\theta - v_r)(1 - \rho))$. In this limit the steady state activity is linear in the mean external driving force μ_e. Moreover, as expected, ν_{steady} is monotonically increasing with the average feedback $J_E C_E(1 - \gamma g) = \rho(\theta - v_r)$ (as long as it is positive, namely, as long as the excitation dominates the inhibition).

- The condition for instability, characterized by the emergence of an oscillatory solution, is $\rho + O\left(\eta^2 + \kappa\eta\right) < -1$, which, in terms of physical parameters, to leading order, corresponds to

$$\frac{J_E C_E(1 - \gamma g)}{\theta - v_r} < -1, \tag{19}$$

  implying that oscillations occur only for a sufficiently large value of inhibition, yielding a strong average negative feedback. This requirement for strong inhibition (or negative feedback in general) is known from many other systems (e.g., (Glass & Mackey, 1988; Murray, 2002)).

- If an oscillatory solution develops, then, to leading order, ν_{old} and ν_{new} alternatingly assume the values 0 and $1 - \eta/2 + O\left(\eta^2 + \eta\kappa\right)$, with short-time transitions in between. Note that during these transitions the term $1 + \rho\nu_{\text{old}}$ changes sign, so the strong-drift assumption (stating that the term multiplying $P(v, t)$ in (6) is large) breaks down during these short time intervals, whereby the system undergoes a fast shift to the next quasi-steady activity. In physical terms, the maximal amplitude of the oscillation is given, to leading order, by

$$\nu_{\max} \approx (\mu_e - (v_r + \theta)/2)/(\tau(\theta - v_r)) \approx (1 - \rho)\nu_{\text{steady}}.$$

- The period of the oscillations tends to 2 as ϵ tends to zero ($2D$ in physical units.)

In Figure 2 we compare the results of the theory to a full accurate numerical solution of the FP equation (6); the details of the numerical solver are provided in Appendix B. The top left figure displays the fixed point iterations for the case where the stationary solution is stable, and the top right figure depicts the dynamical evolution resulting from the numerical solution of the FP equation, converging to the steady solution of $\nu = G(\nu)$. The lower figure displays the case where the stationary solution is unstable, leading to oscillations. The left figure depicts the discrete dynamics $\nu_{\text{new}} = G(\nu_{\text{old}})$ leading to a two-cycle corresponding to the oscillation in the full system, and the right figure presents the oscillations resulting from the solution of the FP equation (6). As can be seen from the figure, the period and amplitude of the oscillations are very well captured by the theory.

The accuracy of the discrete time approximation (14) is further explored in Figure 3 for a range of η values and several values of ϵ. The left plot compares the oscillation amplitude observed in the numerical results to that obtained by setting $\nu_{\rm old} = 0$ on the right side of (18). For the right plot, we differentiate the right side of (18) with respect to $\nu_{\rm old}$, evaluate it at $\nu_{\rm steady}$, obtained also from (18) by setting $\nu_{\rm new} = \nu_{\rm old}$, and equate it to -1. This yields the following theoretical critical value of ρ associated with the onset of instability:

$$\rho_{\rm crit} = -1 - 4\kappa\eta - (12\beta - 1)\eta^2/3 + O(\eta^3 + \kappa\eta^2).$$

We compare this to the critical ρ of the numerical solutions. The figure shows both the great accuracy of the theoretical prediction when ϵ and η are small, and its continuing relevance even when these values are not very small. Observe that, as noted, the tendency towards oscillatory behavior is stronger as $\epsilon \to 0$ (long delay,) and also as $\eta \to 0$ (focused external drive) manifest in the negative slopes of the graphs with respect to each of these parameters.

In summary, we obtain explicit physical estimates for the onset of instability, for the steady activity and for the amplitude and frequency of the oscillations. These computations were possible due to the establishment of the discrete mapping (14), which can be analyzed much more effectively than the full nonlinear PDE (6).

Next, we consider the period of the oscillations, focusing on its dependence on the parameters ϵ, ρ and η. The framework developed does not enable us to obtain expansions for the period, beyond the leading order (in ϵ) term, which is 2 ($2D$ in physical units). We therefore resort to a numerical study, fixing $\beta = \kappa = 0.1$ and compute the period for a range of values of ϵ and for several values of ρ and η. The results are given in Figure 4.

As expected, the nondimensional period tends to 2 as ϵ tends to 0. We discern a clear tendency towards an increase of the period as ϵ is increased, which becomes faster as ρ becomes more negative (more dominant inhibition). We observe four distinct "fans", corresponding to the different values of ρ. Note that the fan 'widths' decrease as ρ becomes more negative. We conclude that, to a first approximation in small ϵ/η, the period is roughly a (linear) function of this parameter ratio:

$$\text{Period} \approx 2 + c\frac{\epsilon}{\eta} = 2 + c\frac{\tau}{D}\,,$$

and this approximation improves rapidly as ρ becomes more negative. In terms of physical units the period is thus approximately $2D + c\tau$, with the slope c increasing as ρ becomes more

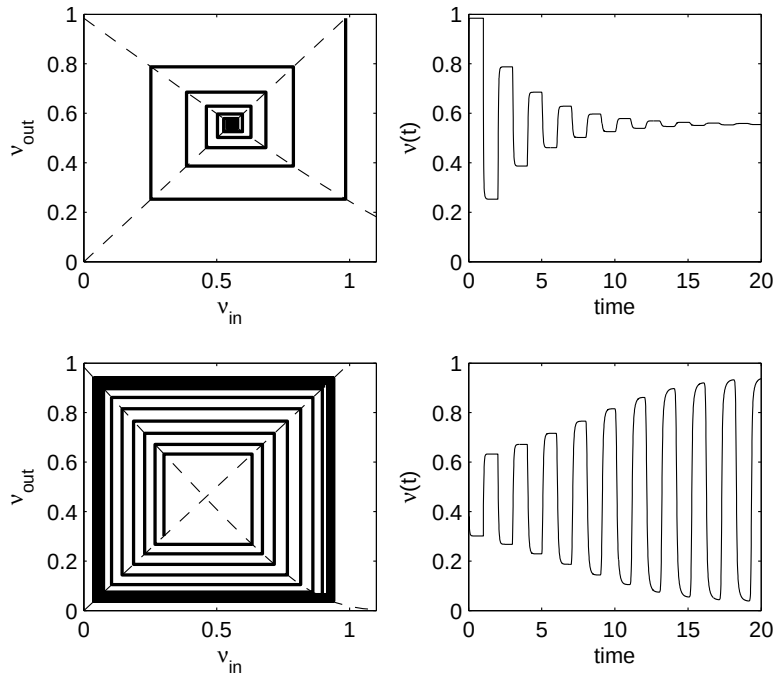

Figure 2: Top left - the function $G(\nu)$ and iterations of (14) leading to a fixed point. Top right - the temporal dynamics based on a numerical solution of the full Fokker-Planck equation. Bottom left and right, same as above, in the oscillatory regime. The parameter values are $\epsilon = 0.01,\ \eta = 0.05,\ \beta = 4,\ \kappa = 0.1$, and $\rho = -0.8$ for the top figure and $\rho = -1.2$ for the bottom figure.

negative. Thus, the increase in the period (over the asymptotic value of twice the delay) is approximately proportional to the time-scale of the membrane, which can be thought of as an adjustment time that is added to the delay, resulting from the non-negligible time (relative to D), which is required for the neuron to reach threshold. This adjustment time increases somewhat for stronger inhibition.

The results presented above provide an explicit characterization of the stationary and oscillatory dynamics of the system in the limit of large delays, corresponding to slow temporal oscillations. Before moving on we present a short comparison of our results to those presented in (Brunel, 2000; Brunel & Hakim, 1999), which served as a motivation to our study. This work considers the same system, and provides a closed form solution in the static case, similarly to (10). In general the value of the stationary activity ν is determined implicitly through the self-consistent numerical solution of a set of equations, and can be written out explicitly only in special limits (e.g., equations (23) and (24) in (Brunel, 2000)). Going

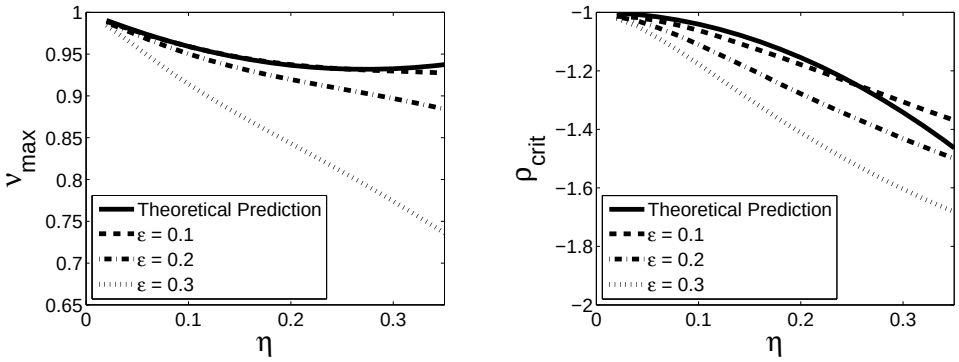

Figure 3: Numerically computed values, based on solving (6), are compared to the theoretical prediction based on the proposed recursion (18) for several values of ϵ and a range of η's, with $\beta = 1$, and $\kappa = 0.01$. Left: oscillation amplitude for $\rho = -2$; Right: ρ_{crit}, the critical value of ρ.

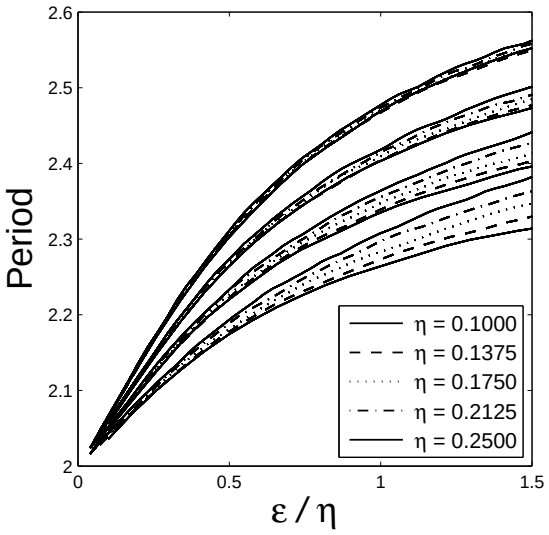

Figure 4: Numerically computed values of the nondimensional period for a range of values of ϵ, with $\beta = \kappa = 0.1$. We observe distinct 'fans', each corresponding to a fixed value of ρ. The values used for ρ are $-1.5, -1.7, -1.9, -2.1$, where -1.5 corresponds to the lowest set of curves and -2.1 to the highest set of curves. The different values of η, within each fan (fixed value of ρ), appear in the figure legend.

beyond the static case, the authors develop a linear stability framework, leading to conditions for the onset of oscillations. This analysis, being perturbative in nature, provides an exact description of the oscillatory behavior only near the bifurcation point. Explicit expressions for the oscillation amplitude, and a complete characterization of the oscillation are difficult

to obtain within such a framework, as was possible in the special limits considered in this work (large delays and/or weak diffusion - see Section 3.2). In fact, the particular oscillatory regime discussed in (Brunel & Hakim, 1999) is restricted to relatively short delays (see Section 3.2 in (Brunel & Hakim, 1999)). In summary, while working within the framework set in (Brunel, 2000; Brunel & Hakim, 1999), we have been able to analytically study a physically interesting regime, not considered explicitly in that work, and for which a great deal of mathematical and physical insight may be obtained regarding the oscillatory mode.

3.2 The regime of low diffusion

A second interesting limit where explicit results can be obtained occurs when the diffusion term in the FP equation (6) is small relative to the term $1+\rho\nu_{\rm old}$, and the delay is not long. More precisely, we let $\kappa \to 0$ and $\eta \to 0$. Unlike other parts of this paper, ϵ need not be small in this limit. This regime corresponds to the left-hand parts in Figure 3, where it is indeed seen that $\nu_{\max} \to 1$ and $\rho_{\rm crit} \to -1$ independently of ϵ. The behavior in this regime differs from that observed in the previous section. Specifically, the oscillatory regime in section 3.1 led to an oscillation taking place between two quasi-stationary regimes (see Figure 2). In the present case the oscillation is more complicated in nature, leading to three different regimes within each oscillation period - see Figure 5.

The FP equation (6) becomes

$$\begin{cases} \epsilon\dfrac{\partial P(v,t)}{\partial t} = -\dfrac{\partial S(v,t)}{\partial v} + \delta(1,t)S(1,t), \\ S(v,t) = -\left[-1-\rho\nu_{old}\right]P(v,t) \\ P(1,t) = 0, \\ P(-\infty,t) = 0, \\ \displaystyle\int_{-\infty}^{1} P(v,t)d\hat{v} = 1. \end{cases} \tag{20}$$

The solution to this diffusion-free equation is of the form

$$P(v,t) = F(\epsilon v - t(1+\rho\nu_{\rm old})), \tag{21}$$

for some smooth function $F(x)$. Such a solution describes a linear dependence of the voltage v on time, augmented by the boundary condition stating that upon reaching $v=1$, the voltage is instantaneously re-injected at $v=0$.

Consider first the case where $-1 \leq \rho \leq 0$. In this case, the flux moves towards $v = 1$ at speed $(1 + \rho)/\epsilon$, and since, upon reaching $v = 1$, it is re-injected at $v = 0$, we obtain a steady solution $P_0(v) = \mathbf{1}[0 \leq v \leq 1]$, where $\mathbf{1}[A]$ is an indicator function which equals 1 on the set A and 0 otherwise.

In the case where $\rho < -1$, a periodic solution of approximate period $1 - \rho$ is obtained consisting of three distinct phases. Without loss of generality, we describe the dynamics of one cycle at the times $0 \leq t \leq 1 - \rho$. The three phases, described below, are depicted graphically in Figure 5. A summary of this dynamics is presented in Figure 5.

Phase 1: $0 \leq t < 1$. We set the time origin to 0 arbitrarily; any other initial point would do. We assume that $\nu(t - 1) = 0$ and $\nu(t) = 1$ in this regime. We will show that after time $2 - \rho$, these conditions are repeated leading to oscillatory behavior. From the conditions $\nu(t - 1) = 0$ and $\nu(t) = 1$ we see that for $0 \leq t < 1$ the flux tends to move to the right with speed $1/\epsilon$, and since it is re-injected at $v = 0$ we obtain the stationary solution $P_0(v) = \mathbf{1}[0 \leq v \leq 1]$. The value $\nu(t) = 1$ is readily found by computing the quasi-steady solution in the limits we are considering here.

Phase 2: $1 \leq t < 2$, $\nu(t - 1) = 1$ and $\nu(t) = 0$. The flux velocity is equal to $(1 + \rho)/\epsilon < 0$. Thus, the square moves to the left, i.e., towards the negative direction of v. During this time, which lasts 1 unit until $\nu(t - 1)$ becomes 0, the square traverses a distance of $|(1 + \rho)/\epsilon|$.

Phase 3: $2 \leq t < 1 - \rho$, $\nu(t - 1) = 0$ and $\nu(t) = 0$. From the previous phase $\nu(t - 1) = 0$. The drift direction is towards the right with speed $1/\epsilon$, i.e., the positive direction of v. This phase lasts until the rectangle reaches the threshold $v = 1$, i.e., $-\rho - 1$ time units.

We demonstrate in Figure 6 that this behavior is indeed approximately reproduced in the numerical solution of the PDE (6), under the conditions specified above (see figure caption for parameter values.) Note that this is not an exact analysis, because $1 + \rho\nu_{\text{old}}$ changes sign when we switch from phase to phase, and the terms that were assumed small actually diverge for a short period of time. This, and the non-vanishing diffusion, are the reason for the smoothing of the square as it travels to the left. However, the square is resharpened when the first phase is repeated, and the limit cycle thus persists.

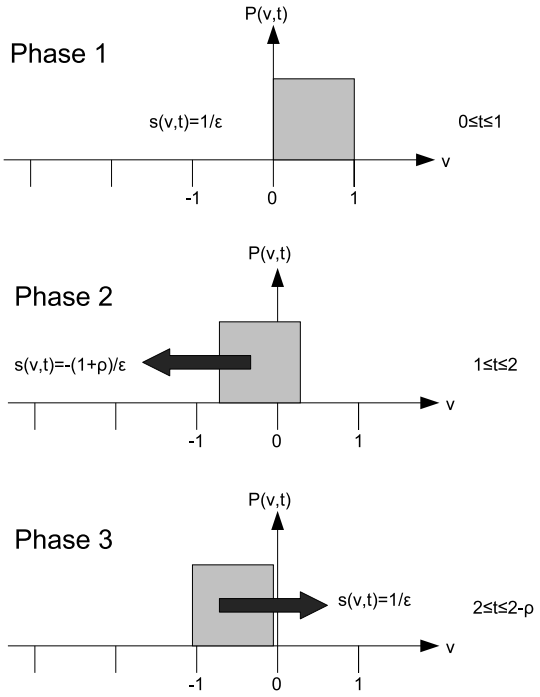

Figure 5: Illustrating the dynamics of the FP equation in the case of small diffusion, where $\kappa \to 0$ and $\eta \to 0$. Following an initial phase with $P(v,t) = \mathbf{1}[0 \leq v \leq 1]$, the distribution moves to the left during phase 2, and then again to the right in phase 3, thereby completing a cycle after time $1 - \rho$. Details of the dynamics are given in the main text.

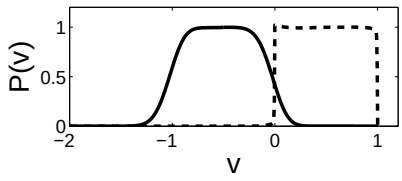

Figure 6: The distribution $P(v,t)$, obtained by a numerical solution of (6), for a moderate value of ϵ but small values of η and κ, displaying the shape at the beginning ($P(v,t) = \mathbf{1}[0 \leq v \leq 1]$) and middle of a cycle (cf. Figure 5). The parameters used are $(\epsilon, \eta, \rho, \beta, \kappa) = (2, 0.002, -5, 1, 0.01)$.

4 Summary and Conclusions

We have studied a sparsely connected network of excitatory and inhibitory spiking neurons influencing each other through delayed interactions. Within the mean field formalism developed in (Brunel, 2000), and captured within a nonlinear FP equation description, we have constructed a simplified description of the dynamics based on a nonlinear discrete time mapping. Focusing on the oscillatory regime, which has mainly been characterized in the past through numerical simulations and linear stability analysis, we have been able to present a closed-form concise description of the oscillations. As has been shown in previous work (e.g., (Brunel & Hakim, 1999; Lindner et al., 2005)), long delays and a strong and focused driving force are conducive to oscillatory behavior. Our work is consistent with this observation, and goes one step further by presenting closed form discrete time approximations to the full dynamics described through the continuous time FP equation. While the formalism provides an almost exact description of the dynamics in the limit of large delays and focused drive, we have shown by careful numerical solutions of the FP equations that they hold across a broad range of parameters, beyond the limit where they are mathematically justified. The approach quantifies the precise degree to which the different system parameters contribute to the emergence of oscillations, thereby quantifying the interplay between internal feedback and external drive required to produce oscillations.

Previous work demonstrated that inhibition contributes to oscillations in networks of spiking neurons. This earlier work focused mainly on two types of regimes. The first, corresponding to a synchronous oscillation mode (e.g., (Vreeswijk, Abbott, & Ermentrout, 1994; Wang & Buzsáki, 1996)), occurs when single neurons fire at a rate which is close to the frequency of the network oscillation; a situation often referred to as spike-to-spike synchronization. The second, so-called irregular mode, takes place when a fast network rhythm is generated, while single neurons fire sparsely and asynchronously (Brunel, 2000;

Brunel & Hakim, 1999, 2008). In both cases the network fires at fast rates, and inhibitory delays do not play a role in the synchronization. The regime described in Section 3.1 is different in that it assumes long delays and leads to slow inhibitory driven oscillations with a period which is much longer than the typical neuronal time scales. Given the complexity and variety of neuronal oscillations (Buzsáki, 2006), there are clearly oscillation regimes for which a theoretical understanding is still lacking.

While it is difficult to conduct physiological experiments which directly address the dependence of oscillation properties on the delay, some early work (Glass, Beuter, & Larocque, 1988) related to human motor behavior with visual feedback is relevant to our results. In this study human subject were asked to maintain a constant finger position relative to a stationary baseline, while increasing time delays (between 40 and 1,500 msec) were introduced in the visual feedback. As the time delay increased periodic behavior is observed, with oscillation periods which were consistently between 2 to 4 times the time delay. This behavior is consistent with our prediction for the dependence of the oscillation period on the temporal delay.

The mathematical analysis of the nonlinear FP equation describing the mean-field behavior of networks of spiking neurons has focused in the past mainly on the steady state and on linear stability analysis. Dealing with the full dynamical behavior is very difficult in general, but can be simplified considerably in appropriate limits, such as the limit considered in this work. The extension of the approach presented here to more realistic situations, e.g., multiple populations, heterogeneous networks, realistic architectures, time-dependent inputs, etc., forms an open research program.

Appendix A: The full asymptotic expansion of G

Denote $h = A/B$. If $h < 1$ and $h/(1-h)^2 < B$, then, after much manipulation, the derivative of P_0 at $v = 1$ can be expanded in a series of the form

$$-\frac{\partial P_0(v,t)}{\partial v}\bigg|_{v=1} = -hB\left[\log(1-h) - \sum_{k=1}^{n}\left(-\frac{h}{B}\right)^k a_k\left[(1-h)^{-2k}-1\right] + O\left(\frac{h}{B(1-h)^2}\right)^{n+1}\right]^{-1},$$

where the coefficients a_k can be computed explicitly, yielding:

$$a_1 = 0.5,\ a_2 = 0.75,\ a_3 = 2.5,\ a_4 = 13.125, \quad \ldots$$

The series of coefficients diverges, however, by taking a finite number of terms we can obtain a highly accurate approximation so long as the term $h/B(1-h)^2$ is small compared to one. Fixing B and expanding in small h, we obtain

$$-\frac{\partial P_0(v,t)}{\partial v}\bigg|_{v=1} = \sum_{k=0}^{m} b_k h^k + O(h^{m+1})\,, \tag{22}$$

with

$$b_0 = B \quad ; \quad b_1 = 1 - \frac{B}{2} \quad ; \quad b_2 = \frac{1}{2} - \frac{2}{B} - \frac{B}{12} \quad ; \quad b_3 = \frac{7}{12} + \frac{10}{B^2} - \frac{3}{B} - \frac{B}{24} \quad ; \quad \cdots$$

Appendix B: The Numerical Solver

Equation (6) is somewhat non-standard, due to the delay and the non-local boundary conditions. This, and the requirement for conservation of the probability, require careful handling. We therefore present a detailed description of the numerical solver for completeness.

The equation is discretized on a mesh of $N_V - 1$ intervals, employing a conserving finite-difference discretization. Although the actual problem extends to $v = -\infty$, the finite-grid approximation can be made as accurate as we wish (due to the fact that the solution decays like a Gaussian as $v \to -\infty$) by employing the following approach. First, we choose some finite minimal value of v, denoted $v_{\min}$, to represent $-\infty$. Then, we replace the boundary condition $P(-\infty, t) = 0$ with the condition $S(v_{\min}, t) = 0$. This allows us to maintain exact conservation of the integral of P (assuming exact arithmetic.) During the solve phase we verify that $P(v_{\min}, t)$ is smaller than some prescribed threshold value at all times, and if it is not, then we extend the domain by reducing v_{min} until this condition is satisfied.

We use k and n to denote the indices along the v and t coordinates, respectively. We employ a uniform grid with mesh-size Δv and time-interval Δt. The discrete probability distribution, $P_{k,n}$, is defined at mesh-points, hence indexed by integer values, $1 \le k \le N_V$, while the flux, S, and the boundary conditions, are defined at interval centers, halfway between mesh-points: $1 < k + \frac{1}{2} < N_V$.

We solve the discretized PDE using an implicit backward-Euler time-stepping scheme (Strikwerda, 2007). This leads to a system that is nearly tridiagonal, but possibly modified slightly due to the nonlocal boundary conditions. Let us write the flux generically as

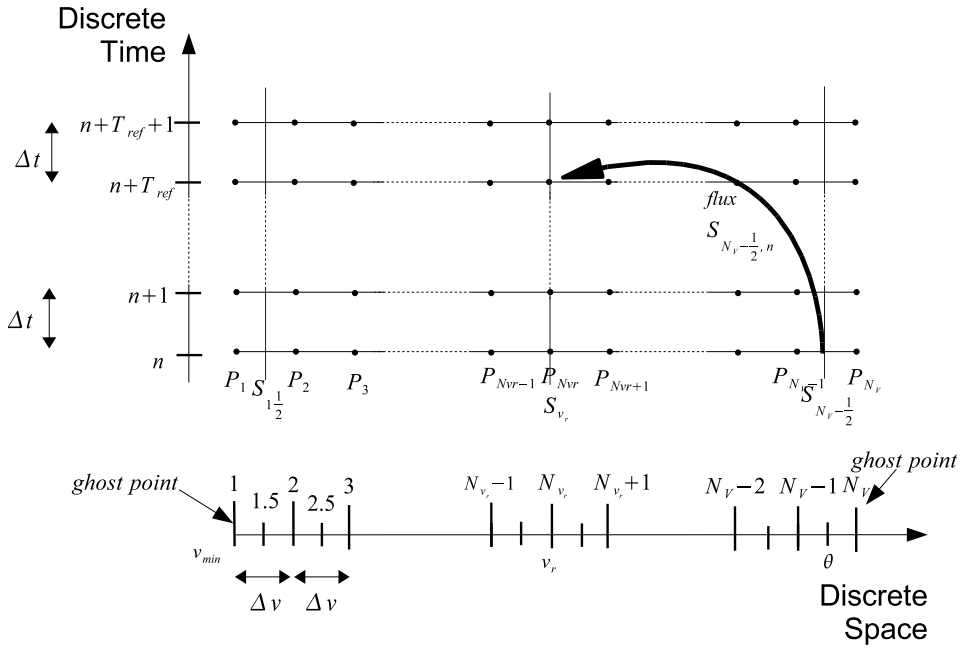

Figure 7: The numerical grid used for the FP equation; see main text for motivation of the scheme, and definitions of the variables.

$$S(v,t) = -\left(F(v,t)P(v,t) + D(t)\frac{\partial}{\partial v}P(v,t)\right),$$

and denote by $F_{k,n}$ as the discrete version of $F(v,t)$ and by D_n the discrete version of $D(t)$. The discrete form of the flux is then given by

$$S_{k+\frac{1}{2},n} = -\left(\frac{D_n(P_{k+1,n}-P_{k,n})}{\Delta v} + F_{k+\frac{1}{2},n}\frac{P_{k+1,n}+P_{k,n}}{2}\right). \tag{23}$$

Except at special points (the ghost points 1 and N_V, that lie just outside the boundaries, and the mesh point N_{V_r} where the outgoing flux is injected), we thus obtain the following scheme:

$$\begin{aligned}\frac{P_{k,n}-P_{k,n-1}}{\Delta t} =& -\left(\frac{S_{k+\frac{1}{2},n}-S_{k-\frac{1}{2},n}}{\Delta v}\right)\\ =& D_n\frac{P_{k+1,n}-2P_{k,n}+P_{k-1,n}}{\Delta v^2}\\ &+ F_{k+\frac{1}{2},n}\left(\frac{P_{k+1,n}+P_{k,n}}{2\Delta v}\right) - F_{k-\frac{1}{2},n}\left(\frac{P_{k,n}+P_{k-1,n}}{2\Delta v}\right),\end{aligned} \tag{24}$$

which leads to the tridiagonal form:

$$\begin{aligned} P_{k,n-1}\frac{1}{\Delta t} =& P_{k-1,n}\left(\frac{F_{k-\frac{1}{2},n}}{2\Delta v} - \frac{D_n}{\Delta v^2}\right) + P_{k,n}\left(\frac{1}{\Delta t} + \frac{2D_n}{\Delta v^2} - \frac{F_{k+\frac{1}{2},n} - F_{k-\frac{1}{2},n}}{2\Delta v}\right) \\ &+ P_{k+1,n}\left(-\frac{D_n}{\Delta v^2} - \frac{F_{k+\frac{1}{2},n}}{2\Delta v}\right). \end{aligned} \tag{25}$$

At the left-hand boundary, we apply the condition

$$S_{1+\frac{1}{2},n} = 0\,, \tag{26}$$

which yields

$$P_{1,n}\left(-\frac{F_{1+\frac{1}{2},n}}{2\Delta v} + \frac{D_n}{\Delta v^2}\right) + P_{2,n}\left(-\frac{F_{1+\frac{1}{2},n}}{2\Delta v} - \frac{D_n}{\Delta v^2}\right) = 0\,.$$

The vanishing of P at the right-hand boundary is discretized by

$$\frac{P_{N_V-1,n} + P_{N_V,n}}{2} = 0.$$

Finally, we need to compute the outgoing flux and re-inject it at mesh-point N_{V_r} after time lag τ_{ref}. Using (23), the discrete outgoing flux is given by

$$\begin{aligned} S_{N_V-\frac{1}{2},n} =& -\left(D_n\frac{P_{N_V,n} - P_{N_V-1,n}}{\Delta v} + F_{N_V-\frac{1}{2},n}(P_{N_V,n} + P_{N_V-1,n})\right) \\ =& P_N\left(-\frac{D_n}{\Delta v} - F_{N_V-\frac{1}{2},v}\right) + P_{N_V-1,n}\left(+\frac{D_n}{\Delta v} - F_{N_V-\frac{1}{2},n}\right). \end{aligned} \tag{27}$$

Finally, we modify (25) at the mesh-point N_{V_r} to reflect the injection of the flux,

$$\begin{aligned} &P_{N_{V_r}-1,n}\left(\frac{F_{N_{V_r}-\frac{1}{2},n}}{2\Delta v} - \frac{D_n}{\Delta v^2}\right) + P_{N_{V_r},n}\left(\frac{1}{\Delta t} + \frac{2D_n}{\Delta v^2} - \frac{F_{N_{V_r}+\frac{1}{2},n} - F_{N_{V_r}-\frac{1}{2},n}}{2\Delta v}\right) + \\ &P_{N_{V_r}+1,n}\left(-\frac{D_n}{\Delta v^2} - \frac{F_{N_{V_r}+\frac{1}{2},n}}{2\Delta v}\right) = P_{N_{V_r},n-1}\frac{1}{\Delta t} + \frac{1}{\Delta v}S_{N-\frac{1}{2},\,n-\frac{\tau_{ref}}{\Delta t}}\,, \end{aligned} \tag{28}$$

where we have assumed that τ_{ref} is an integer multiple of Δt. Note that in the special case of $\tau_{ref} = 0$ the resulting system is not longer tridiagonal. However, its solution requires only a slight modification of the classical highly efficient Thomas algorithm for tridiagonal systems.

Beginning with prescribed initial conditions, the numerical solution is computed by solving a simple linear system per time level. It is easy to verify that the discretization conserves (in exact arithmetic) the sum of $P_{k,n}$ over the internal part of the domain for all n. Of course the initial conditions are prescribed such that this sum times ΔV is equal to 1.

Acknowledgment The work of RM was partially supported by a Converging Technologies grant from the Israel Science Foundation.

References

Börgers, C., & Kopell, N. (2003). Synchronization in networks of excitatory and inhibitory neurons with sparse, random connectivity. *Neural Comput*, *15*(3), 509–538.

Brunel, N. (2000). Dynamics of sparsely connected networks of excitatory and inhibitory spiking neurons. *8(3)*, 183-208.

Brunel, N., & Hakim, V. (1999). Fast global oscillations in networks of integrate-and-fire neurons with low firing rates. *Neural Comput*, *11*(7), 1621-71.

Brunel, N., & Hakim, V. (2008). Sparsely synchronized neuornal oscillations. *Chaos*, *18*, 015113.

Buzsáki, G. (2006). *Rhythms of the brain*. Oxford University Press.

Buzsáki, G., & Draguhn, A. (2004). Neuronal oscillations in cortical networks. *Science*, *304*(5679), 1926–1929.

Cortes, J. M., Torres, J. J., Marro, J., Garrido, P. L., & Kappen, H. J. (2006). Effects of fast presynaptic noise in attractor neural networks. *Neural Comput*, *18*, 614–633.

Destexhe, A., Contreras, D., & Steriade, M. (1998). Mechanisms underlying the synchronizing action of corticothalamic feedback through inhibition of thalamic relay cells. *J Neurophysiol*, *79*(2), 999–1016.

Ferster, D., & Lindström, S. (1983). An intracellular analysis of geniculo-cortical connectivity in area 17 of the cat. *J Physiol*, *342*, 181–215.

Gerstner, W., & Kistler, W. (2002). *Spiking neuron models*. Cambridge University Press.

Glass, L., Beuter, A., & Larocque, D. (1988). Time delays, oscillations, and chaos in physiological control systems. *Mathematical Biosciences*, *90*, 111-125.

Glass, L., & Mackey, M. (1988). *From clocks to chaos*. Princeton University Press.

Harvey, A. (1980). A physiological analysis of subcortical and commissural projections of areas 17 and 18 of the cat. *J Physiol*, 507-534.

Hill, S., & Tononi, G. (2005). Modeling sleep and wakefulness in the thalamocortical system. *J Neurophysiol*, *93*(3), 1671–1698.

Lindner, B., Doiron, B., & Longtin, A. (2005). Theory of oscillatory firing induced by spatially correlated noise and delayed inhibitory feedback. *Phys Rev E Stat Nonlin Soft Matter Phys*, *72*, 061919.

Marinazzo, D., Kappen, H., & Gielen, S. (2007). Input-driven oscillations in networks with excitatory and inhibitory neurons with dynamic synapses. *Neural Comput*, *19*(7), 1739–1765.

Miller, R. (1996). Cortico-thalamic interplay and the security of operation of neural assemblies and temporal chains in the cerebral cortex. *Biol Cybern*, *75*, 263–275.

Murray, J. D. (2002). *Mathematical biology* (Third ed.). Springer.

Renart, A., Brunel, N., & Wang, X. (2003). In J. Feng (Ed.), *Computational neuroscience: A comprehensive approach* (p. 432-490). CRC Press.

Risken, H. (1996). *The fokker-planck equation: Methods of solutions and applications* (Second ed.). Springer.

Roxin, A., Brunel, N., & Hansel, D. (2005). Role of delays in shaping spatiotemporal dynamics of neuronal activity in large networks. *Phys Rev Lett*, *94*(23), 238103.

Strikwerda, J. C. (2007). *Finite difference schemes and partial differential equations* (Second ed.). SIAM.

Strogatz, S. (2001). *Nonlinear dynamics and chaos: with applications to physics, biology, chemistry and engineering*. Perseus Books Group.

Swadlow, H. A. (1991). Efferent neurons and suspected interneurons in second somatosensory cortex of the awake rabbit: receptive fields and axonal properties. *J Neurophysiol*, *66*, 1392–1409.

Tuckwell, H. (1989). *Stochastic processes in the neurosciences*. SIAM.

Vogels, T., Rajan, K., & Abbott, L. (2005). Neural network dynamics. *Annu. Rev. Neurosci.*, *28*, 357-376.

Vreeswijk, C. V., Abbott, L. F., & Ermentrout, G. B. (1994). When inhibition not excitation synchronizes neural firing. *J Comput Neurosci*, *1*(4), 313–321. (n1224)

Wang, X., & Buzsáki, G. (1996). Gamma oscillation by synaptic inhibition in a hippocampal interneuronal network model. *J Neurosci.*, *16(20)*(4), 6402-13. (n1224)

White, J. A., Chow, C. C., Ritt, J., Soto-Trevio, C., & Kopell, N. (1998). Synchronization and oscillatory dynamics in heterogeneous, mutually inhibited neurons. *J Comput Neurosci*, *5*(1), 5–16.